materials

MDPI

Article

Comparative Study of the Adsorption of Acid Blue 40 on Polyaniline, Magnetic Oxide and Their Composites: Synthesis, Characterization and Application

Amir Muhammad [1], Anwar ul Haq Ali Shah [1,*] and Salma Bilal [2,3,*]

[1] Institute of Chemical Sciences, University of Peshawar, Peshawar 25120, Pakistan
[2] National Centre of Excellence in Physical Chemistry, University of Peshawar, Peshawar 25120, Pakistan
[3] TU Braunschweig Institute of Energy and Process Systems Engineering, Franz-Liszt-Straße 35, 38106 Braunschweig, Germany
* Correspondence: anwarulhaqalishah@uop.edu.pk (A.u.H.A.S.); s.bilal@tu-braunschweig.de or salmabilal@uop.edu.pk (S.B.); Tel.: +92-919216652 (A.u.H.A.S.); +49-531-39163651 or +92-919216766 (S.B.)

Received: 24 July 2019; Accepted: 31 August 2019; Published: 4 September 2019

Abstract: Conducting polymers (CPs), especially polyaniline (PANI) based hybrid materials have emerged as very interesting materials for the adsorption of heavy metals and dyes from an aqueous environment due to their electrical transport properties, fascinating doping/de-doping chemistry and porous surface texture. Acid Blue 40 (AB40) is one of the common dyes present in the industrial effluents. We have performed a comparative study on the removal of AB40 from water through the application of PANI, magnetic oxide (Fe_3O_4) and their composites. Prior to this study, PANI and its composites with magnetic oxide were synthesized through our previously reported chemical oxidative synthesis route. The adsorption of AB40 on the synthesized materials was investigated with UV-Vis spectroscopy and resulting data were analyzed by fitting into Tempkin, Freundlich, Dubinin–Radushkevich (D–R) and Langmuir isotherm models. The Freundlich isotherm model fits more closely to the adsorptions data with R^2 values of 0.933, 0.971 and 0.941 for Fe_3O_4, PANI and composites, respectively. The maximum adsorption capacity of Fe_3O_4, PANI and composites was, respectively, 130.5, 264.9 and 216.9 mg g^{-1}. Comparatively good adsorption capability of PANI in the present case is attributed to electrostatic interactions and a greater number of H-bonding. Effect of pH of solution, temperature, initial concentration of AB40, contact time, ionic strength and dose of adsorbent were also investigated. Adsorption followed pseudo-second-order kinetics. The activation energy of adsorption of AB40 on Fe_3O_4, PANI and composites were 30.12, 22.09 and 26.13 kJmol^{-1} respectively. Enthalpy change, entropy change and Gibbs free energy changes are −6.077, −0.026 and −11.93 kJ mol^{-1} for adsorption of AB40 on Fe_3O_4. These values are −8.993, −0.032 and −19.87 kJ mol^{-1} for PANI and −10.62, −0.054 and −19.75 kJ mol^{-1} for adsorption of AB40 on PANI/Fe_3O_4 composites. The negative sign of entropy, enthalpy and Gibbs free energy changes indicate spontaneous and exothermic nature of adsorption.

Keywords: Acid blue 40 dye; adsorption isotherms; kinetics and thermodynamic study

1. Introduction

The discovery of conducting polymers in 1977 initiated an interesting field of research. These polymers showcased fascinating physico-chemical properties which made them suitable for numerous applications [1]. Polyaniline, polythiophene, polypyrrole and their derivatives are the most studied conducting polymers [2–5] and show optical as well as conducting properties due to the presence of π conjugated electrons in their skeleton [6]. Polyaniline (PANI) has gained a lot interest

among the conducting polymers family because it can be synthesized easily from low-cost materials. It is highly conductive and possesses good environmental stability [3,7,8].

A number of methods including chemical oxidation, electro-chemical oxidation, enzymatic, interfacial, self-assembling and seeding methods have been applied to synthesize PANI [9–13]. Chemical and electro-chemical oxidation methods are the most common methods which involve the polymerization of aniline in an acidic or basic medium. However, the conducting emeraldine form of PANI is usually synthesized in an acidic environment [14]. PANI has been effectively applied in corrosion protection, batteries, solar cells, supercapacitors and adsorption of heavy metals and dyes from an aqueous solution [3,15–18]. The suitability of PANI as an adsorbent to remove dyes from an aqueous environment is due to the presence of a large number of amine and imine functional groups which are expected to interact with dyes. The charge transfer induced by doping enables PANI to interact with ionic species through electrostatic interactions [19]. Although PANI has been used widely as an adsorbent for the removal of dyes from water, its performance is restricted due to two main challenges. Firstly, its particles aggregate due to intermolecular interactions, resulting in the decrease of surface area and hence the adsorption capacities [20]. Secondly, acid doped PANI is prone to de-doping due to the evaporation of the small acid molecules at room temperature. This causes a reduction in the surface charge of PANI which ultimately affect the electrostatic interaction between PANI and dye [21].

To overcome these challenges, considerable work has been done in recent years to synthesize composites of PANI with inorganic substances such as Ag, Cd, SiO_2, TiO_2, ZnO, MnO_2 and magnetic oxide (Fe_3O_4) [22–25]. These composites exhibit characteristics electrical, optical, catalytic and mechanical properties that are better than single components in some cases. The composites of PANI and Fe_3O_4 have attracted much attention because of easy synthesis and numerous applications in areas such as in biosensors, sensors, solar cells and purification of water [26–29].

Just like PANI, magnetic oxide also finds applications in drug delivery systems [30], clinical diagnosis [31], efficient hyperthermia for the removal of cancer [32], microwave devices, magnetic resonance imaging (MRI) [33,34] and the removal of heavy metals from an aqueous solution [35,36]. Electric explosion of wire, laser target evaporation and biomineralization are commonly used for controlled size and morphology of Fe_3O_4 [37], but the wet chemical methods, like the chemical co-precipitation method [38], sol-gel [39], hydrothermal method [40], gas phase [41], liquid phase [42] and two-phase methods such as microemulsion methods [43] are also used for the preparation of Fe_3O_4.

In general, composites of PANI and Fe_3O_4 have been synthesized either through in situ formations of magnetic oxide composites in the presence of PANI [44] or polymerization of aniline monomers in the presence of iron oxide. In comparison with the former, the latter strategy gives better results because of the magnetic properties of the resulting hybrid materials [45].

Bhaumik et al. [46] prepared nanofibers composites from metallic nanoparticles and PANI and applied these composites to remove arsenic (V), chromium (VI) and Congo red from an aqueous solution. Different polymer salts (PANI–HNO_3, PANI–H_2SO_4 and PANI–H_3PO_4) are reported to use as adsorbents to remove Direct Blue 78 (DB78) from water [47]. The dye uptake was in the order PANI–H_3PO_4 > PANI–H_2SO_4 > PANI–HNO_3. The rate of adsorption was decreased as the concentration of DB78 and pH of dye solution increased. The adsorption followed pseudo-second-order kinetics. Cui and co-workers [48], studied the adsorption of Hg (II) onto polyaniline/attapulgite (PANI/ATP) composites. (PANI/ATP) composites were synthesized by the chemical oxidation method. The maximum amount of dye adsorbed was 800 mg/g when the pH of Hg (II) solution was 5.9 and followed pseudo-second-order kinetics.

In the present study, PANI/Fe_3O_4 is used as an adsorbent to remove Acid Blue 40 (AB40) from water. The adsorption behaviors of PANI/Fe_3O_4 were compared with PANI and Fe_3O_4 which were synthesized and tested according to our previous work [49]. The chemical oxidation method was used to synthesize PANI and PANI/Fe_3O_4 composites using $FeCl_3{\cdot}6H_2O$ as an oxidant in an acidic medium, while the chemical co-precipitation method was adopted to synthesize Fe_3O_4 materials in

the basic medium at a temperature of 85–90 °C. All these synthesized materials were characterized through UV-Vis, SEM, FTIR, EDX and surface area measurements. Adsorption study was carried out to determine the effect of pH, initial concentration, temperature, contact time, adsorbent dosage and ionic strength on adsorption phenomenon using UV-Vis spectroscopy. Freundlich, Langmuir, D–R and Tempkin adsorption isotherm models were applied to analyze the adsorption data. The adsorption mechanism was determined on the basis of kinetic study. Thermodynamic aspects of adsorption of AB40 on these materials were also investigated.

2. Experiment

2.1. Materials

Aniline was purchased from Across and distilled under vacuum. Acid Blue 40 dye, $FeCl_3{\cdot}6H_2O$ and Na_2SO_4 (Sigma-Aldrich, St. Louis, MO, USA), Dodecyl benzene sulfonic acid (DBSA) (Across) and $FeSO_4{\cdot}7H_2O$ (Merck, Kenilworth, NJ, USA) were used without further purification.

2.2. Synthesis of PANI

PANI was synthesized via our previously reported chemical oxidation method [49]. Typically, 0.02 M (1.182 mL) aniline was suspended in 50 mL of 0.01 M H_2SO_4 solution. To this suspension 0.01 M (0.15 mL) DBSA was added as an emulsifying agent. Then 50 mL of 0.01 M $FeCl_3{\cdot}H_2O$ prepared in 0.01 M H_2SO_4 was added drop by drop as an oxidant with constant stirring. After 20 min of continuous stirring, a milky white color suspension turned to light green and then dark green in one hour. The final product was thoroughly washed with acetone and then with double-distilled water until the filtrate became clear. The obtained powder was dried in an oven for 24 h at 60 °C.

2.3. Synthesis of Fe_3O_4

Fe_3O_4 was synthesized by the chemical co-precipitation method by adding 0.15 mL DBSA and 2 M of $FeCl_3{\cdot}6H_2O$ dissolved in 50 mL of 0.1 M NaOH to 0.5 M $FeSO_4{\cdot}7H_2O$ solution. The whole mixture was stirred continuously at 85–90 °C. After 20 min of stirring, 30 mL of 5 M ammonia solution was added at once which turned the color of the reacting mixture to black. The pH of the reacting mixture was kept at 10 during the whole experiment. After two hours of continuous stirring at 85–90 °C, the precipitate was washed with ethanol and double distilled water until the effluent became clear. The black precipitate was dried at 80 °C for 10 h and then annealed at 600 °C for 5 h in a furnace (NEYCRAFT JFF 2000 Fiber Furnace, France).

2.4. Synthesis of PANI/Fe_3O_4 Composites

PANI/Fe_3O_4 composites were synthesized by suspending 0.15 g Fe_3O_4 particles in 30 mL of 0.01 M H_2SO_4 solution followed by addition of 50 mL (0.02 M) of aniline solution prepared in 0.01 M H_2SO_4 and 0.5 mL (0.01) DBSA, respectively. After 30 min of continuous stirring, 50 mL of 0.01 M $FeCl_3{\cdot}6H_2O$ was added as an oxidizing agent. A light green color appeared within the stirring mixture after 20 min of the oxidant's addition. The color of this mixture turned dark black after about one hour. After continuously stirring for 6 h, the product was separated and washed with acetone and double-distilled water. The clean precipitate was dried in oven at 60 °C for 24 h.

2.5. Batch Adsorption Study for Removal of AB40 Dye

Twenty-milliliter solutions of different concentrations between 5–120 mgL^{-1} were prepared from the stock solution of AB40 dye. To these solutions, PANI was added and shacked for about 120 min. These solutions were then filtered to determine the concentration of dye in the filtrate using UV-Visible spectrophotometer and applying Equation (1) [50].

$$q_e = \frac{(C_i - C_e)V}{m} \quad (1)$$

where q_e (mg g^{-1}) refers to adsorption at equilibrium, C_i (mg L^{-1}) and C_e (mg L^{-1}) show initial and equilibrium concentration of dye, respectively, m (g) is the mass of adsorbent while V represents the volume of solution in mL. The effect of temperature, contact time, ionic strength, pH and initial concentration of dye solution on the adsorption behavior was studied. The adsorption data were utilized to calculate the thermodynamic and kinetics parameters. The same procedure was employed for studying adsorption of AB40 on Fe_3O_4 and PANI/Fe_3O_4 composite.

Before the adsorption process, standard solutions of AB40 dye were prepared was in the range 0.005–2 mg L^{-1} and their maximum absorption was determined via UV-Visible spectrophotometer (Perkin Elmer, Waltham, MA, USA). The absorption values were plotted against concentration of the standard dye solutions and calibration curve was obtained according to the Beer–Lambert law. The slope so obtained was used as reference for the determination of concentration in rest of the experiments. The calibration curve is also shown in the supporting files (Figure S1).

After the adsorption of AB40 dye, the adsorbents were put onto the filter paper and washed several times with double-distilled water to run out the adsorbed dye. Then it was washed with 0.1 M NaOH to remove the remaining dye. This process enables the reutilization of the adsorbent.

2.6. Characterization

FTIR spectra of the synthesized materials were registered in the spectral range of 400 to 4000 cm^{-1} through a Fourier transmission infrared spectrophotometer (Shimadzu, Tokyo, Japan). X-ray diffraction (XRD) patterns were recorded by using Cu Kα radiations of wavelength 1.5405 Å with the help of a JEOL JDX-3532 (JEOL, Tokyo, Japan). The concentration of dye in the solution and its adsorbed amount onto the synthesized materials were checked through UV-visible spectrophotometer (Perkin Elmer, Buckinghamshire, UK). An energy-dispersive X-ray (EDX) spectrophotometer (Inca 200, Oxford, UK) was utilized to determine the percentage of different elements. Brunauer–Emmett–Teller (BET) surface areas of the composite as well as PANI and Fe_3O_4, were determined in the N_2 atmosphere through adsorption–desorption method with a surface area analyzer model 2200 e Quanta Chrome (Quanta Chrome, Boynton Beach, FL, USA). The surface morphologies were studied through scanning electron microscopy (SEM) (JSM-6490, JEOL, Tokyo, Japan).

3. Results and Discussion

3.1. Scanning Electron Microscopy (SEM)

SEM images provide interesting information about surface morphology and size of adsorbent materials under investigation. Figure 1a,b shows SEM images of Fe_3O_4 particles before and after adsorption of AB40 dye. The Fe_3O_4 particles are round in shape with an average size of 0.15 μm. After adsorption of AB40, the porosity decreases in the agglomerated surface of Fe_3O_4 but the average particles size increases to 0.23 μm (Figure 1b). Keyhanian et al. [50] have reported the agglomeration of magnetic particles of Fe_3O_4 after adhering of methyl violet dye from an aqueous solution.

Rods- or wires-like porous structure can be seen in the SEM image of PANI with 0.21 μm average diameter of the rods (Figure 1c). These rods are aggregated to each other like fibers. After the adsorption of AB40 (Figure 1d), the morphology of PANI changes to a cauliflower shape with some needle-like structures present on the surface. Such a change in morphology was also reported during the adsorption of anionic dyes on PANI doped with Potash Alum [51]. Figure 1e shows an SEM image of PANI/Fe_3O_4 composites. It shows a porous morphology where Fe_3O_4 particles have adhered with PANI interconnected rods. Similar morphology was depicted by nanocomposites of PANI/ Fe_3O_4 coated on $MnFe_2O_4$ [52]. Just like PANI, morphology of PANI/Fe_3O_4 composites also changes after the adsorption of AB40. The dye distributes homogeneously over the surface of composite imparting a broccoli-like appearance to it as shown in Figure 1f.

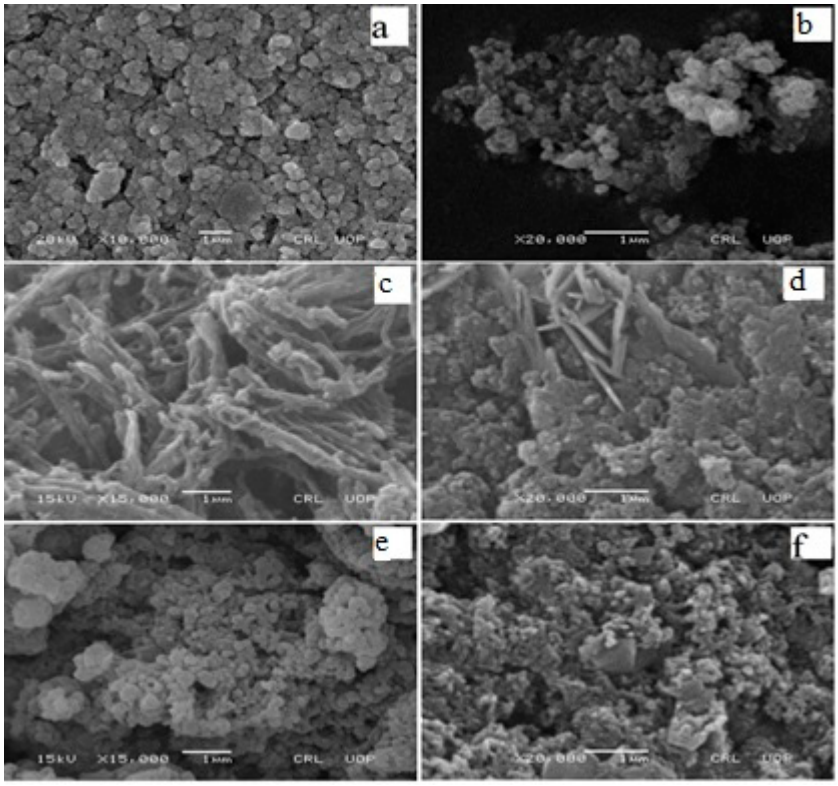

Figure 1. SEM images of magnetic oxide (Fe_3O_4), polyaniline (PANI) and PANI/Fe_3O_4 composite before (**a**,**c**,**e**) and after (**b**,**d**,**f**) adsorption of acid blue 40 (AB40) dye.

3.1.1. Optical Studies

Figure 2A represents the UV-Vis spectra of the synthesized materials before adsorption of the dye. A weak band in the region of 450 nm arises due to the interaction of electromagnetic radiations with the valence electrons of iron in the Fe_3O_4. As a result, the valence electron of the metal atom starts to oscillate with the frequency of the electromagnetic source [53]. This phenomenon is known as surface plasmon resonance (SPR). Another band at 485.85 nm is due to the presence of DBSA moiety with Fe_3O_4 and closely resembles already reported work [54]. The two characteristic bands of PANI can be observed in its spectrum at 333.91 and 633.42 nm. The band at 633.42 nm is due to charge transfer from the benzenoid ring to the quinoid ring and the band at 333.91 nm is attributed to π-π^* transitions of the benzenoid ring [55]. In the spectrum of PANI/Fe_3O_4 composites, the band at 333.91 nm shows a redshift due to the doping of the benzenoid amine with Fe_3O_4 particles. Moreover, the bipolaron band at 633.42 nm is shifted to 773.14 nm suggesting that some physical interactions between PANI and Fe_3O_4 particles may exist [56].

Figure 2B represent UV-visible spectra of Fe_3O_4, PANI and composite of Fe_3O_4 with PANI after adsorption of AB40. One can observe a band in the region of 618–620 nm in all the spectra of Fe_3O_4, PANI and composite of Fe_3O_4 and PANI which indicates the adsorption of AB40. This band has been demonstrated that AB40 shows strong absorption at 620 nm [57]. The intensity of this band is higher for PANI, which is different from our previous work where more intense peaks, due to adsorption of Basic Blue 3 dye, was observed in the spectrum of PANI/Fe_3O_4 composite [49]. The reason can be explained by the fact that in the PANI/Fe_3O_4 composite, the positively charged active sites of PANI are covered by Fe_3O_4. Moreover, the oxygen of Fe_3O_4 behave as negatively charged sites, which may cause repulsion to the negative charge of the anionic dye and hence reduces its adsorption.

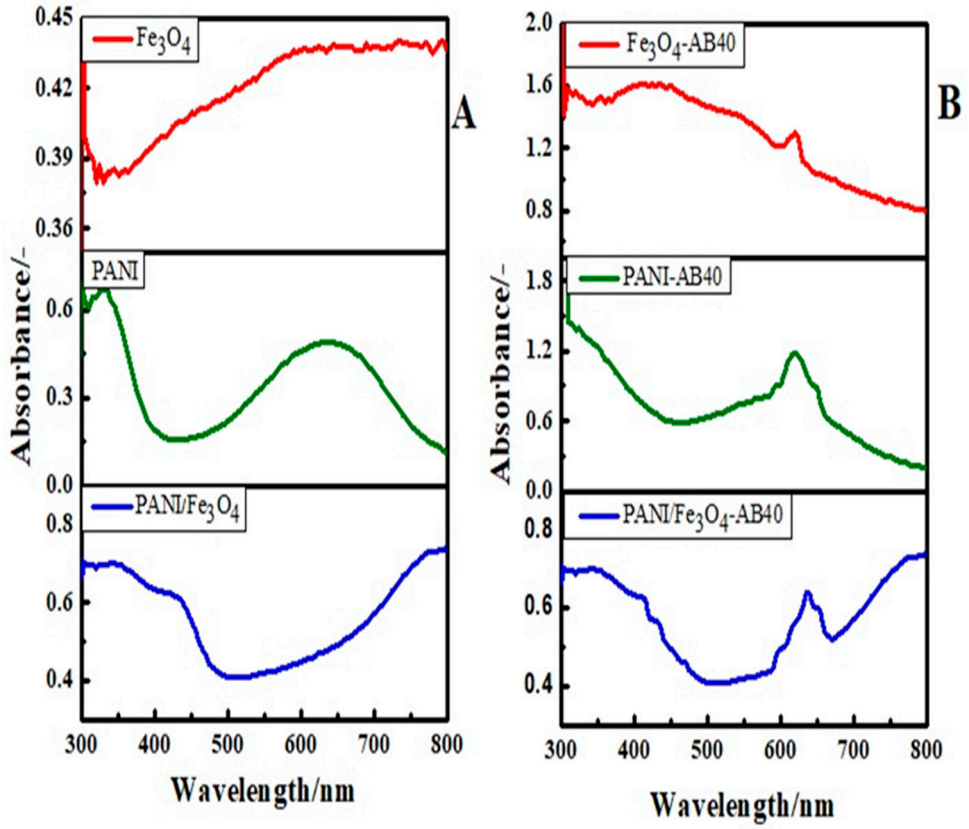

Figure 2. UV-visible spectrum of Fe_3O_4, PANI and PANI/ Fe_3O_4 composite (**A**) before and (**B**) after adsorption of AB40.

3.1.2. Energy Dispersive X-ray (EDX) Study

Figure 3 shows the EDX analysis of PANI, Fe_3O_4 and PANI/Fe_3O_4 composites before and after adsorption of AB40. The weight percent of Fe and O in Fe_3O_4 is 68.74 and 29.15, respectively. After the adsorption of AB40, the weight percent of Fe decreases from 68.74 to 62.09, while the percent weight of O and C increases due to the presence of oxygen and carbon in the AB40 texture. Similarly, the appearance of nitrogen and Sulphur in spectrum 3b is more evidence of the adsorption of AB40 onto Fe_3O_4, as these elements are present in the dye texture [58]. Figure 3c shows the EDX spectrum of PANI before adsorption of AB40. One can observe a 9.54 percent nitrogen and 68.06 percent carbon by weight in this spectrum. The presence of sulfur and oxygen may be due to the presence of DBSA while Fe and Cl may be due to the presence of $FeCl_3 \cdot H_2O$ which was used as oxidant. After adsorption of AB40, although weight percent of carbon decreases but weight percent of nitrogen and oxygen increases which shows that AB40 adsorb on PANI (Figure 3d) [59]. In the EDX spectrum of PANI/Fe_3O_4 composite, peaks for nitrogen, oxygen, carbon and iron can clearly be observed in Figure 3e, confirming the formation of composites. The sulfur percent by weight is 2.66 and is due to the presence of some moiety of DBSA. After the adsorption of AB40, the weight percent of carbon, nitrogen and sulfur is increased (Figure 3f) [60].

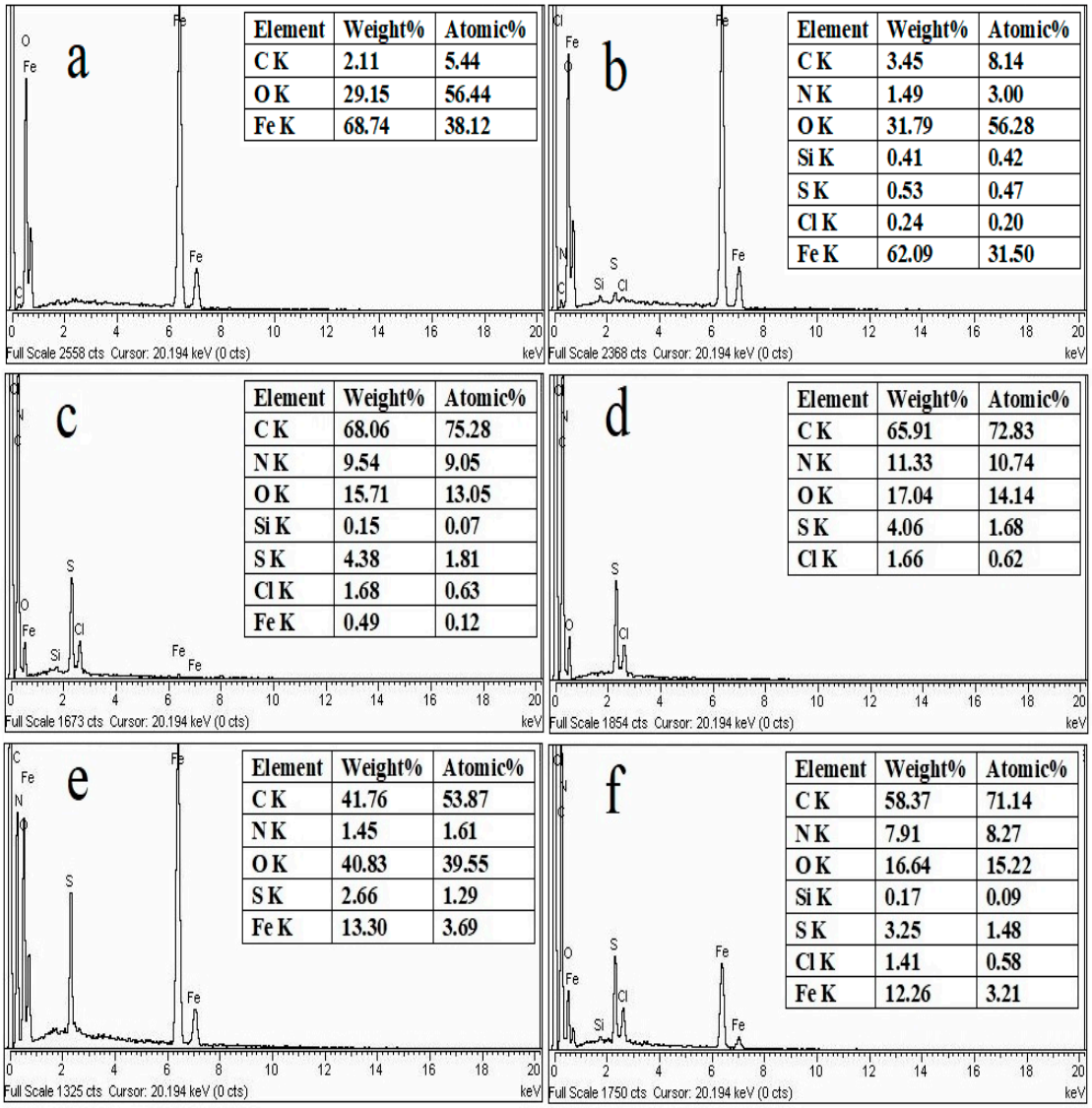

Figure 3. EDX spectra of Fe_3O_4, PANI and PANI/Fe_3O_4 composites before (**a**,**c**,**e**) and after (**b**,**d**,**f**) adsorption of AB40.

3.1.3. FTIR Study

Figure 4A,B represent, respectively, FTIR spectra of Fe_3O_4, PANI and PANI/Fe_3O_4 composite before and after adsorption of AB40. The peak located at 543.1 cm^{-1} is due to the stretching vibration of the Fe–O bond in the Fe_3O_4 spectrum [61]. A wide peak at 3427.34 cm^{-1} shows stretching vibrations of –OH group attached to Fe_3O_4 surface [62]. The shifting of all peaks towards a lower frequency and the appearance of a very small peak at 2343.2 cm^{-1} in Figure 4B indicates that the AB40 dye comes in contact with Fe_3O_4 after adsorption [9,63].

FTIR spectrum of PANI shows –N–H group of secondary amine at 3231.5 cm^{-1}. Similarly, the peaks at 2842.8 and 2932.8 cm^{-1} can be attributed to the symmetric and asymmetric stretching vibrations of the C–H bond, respectively. Vivekanandan et al. have reported such asymmetric and symmetric C–H stretching vibrations at 2923.62 and 2825.55 cm^{-1}, respectively [9]. Peaks at 1602.8 and 1469.3 cm^{-1} attribute to C=C and C=N stretching vibrations of the benzenoid and quinoid rings. The band at 1304.2 cm^{-1} corresponds to the $–C–N^+$ stretching vibrations of the secondary aromatic amine. Similarly, the peaks at 1140.3 and 826.5 cm^{-1} represent the bending vibrations of the aromatic C–H bond in plane and out of plane deformation [64]. The peak at 1020.4 cm^{-1} shows the S=O stretching vibrations of

the –SO_3H group, confirming the presence of DBSA moiety in the PANI texture [65,66]. The peak at 677.2 cm^{-1} shows the out of plane bending vibrations of the C–H bond.

In the spectrum of PANI/Fe_3O_4 composites, all peaks are shifted to the low-frequency range in comparison with PANI, indicating a presence of some physical forces between PANI and Fe_3O_4 particles. The appearance of the small peak at 542.7 cm^{-1} shows Fe-O stretching, which confirms the formation of PANI/Fe_3O_4 composites [67]. After the adsorption of AB40, there is a slight shift of peaks towards a low frequency, both in the spectrum of PANI and PANI/Fe_3O_4 composites. Moreover, the appearance of the peak at 2356.7 cm^{-1} shows the adsorption of AB40 dye on PANI and PANI/Fe_3O_4 composites [68]. This peak is more intense in the spectrum of AB40 adsorbed on PANI as compared to the PANI/Fe_3O_4 composite which is in agreement with the UV-visible study.

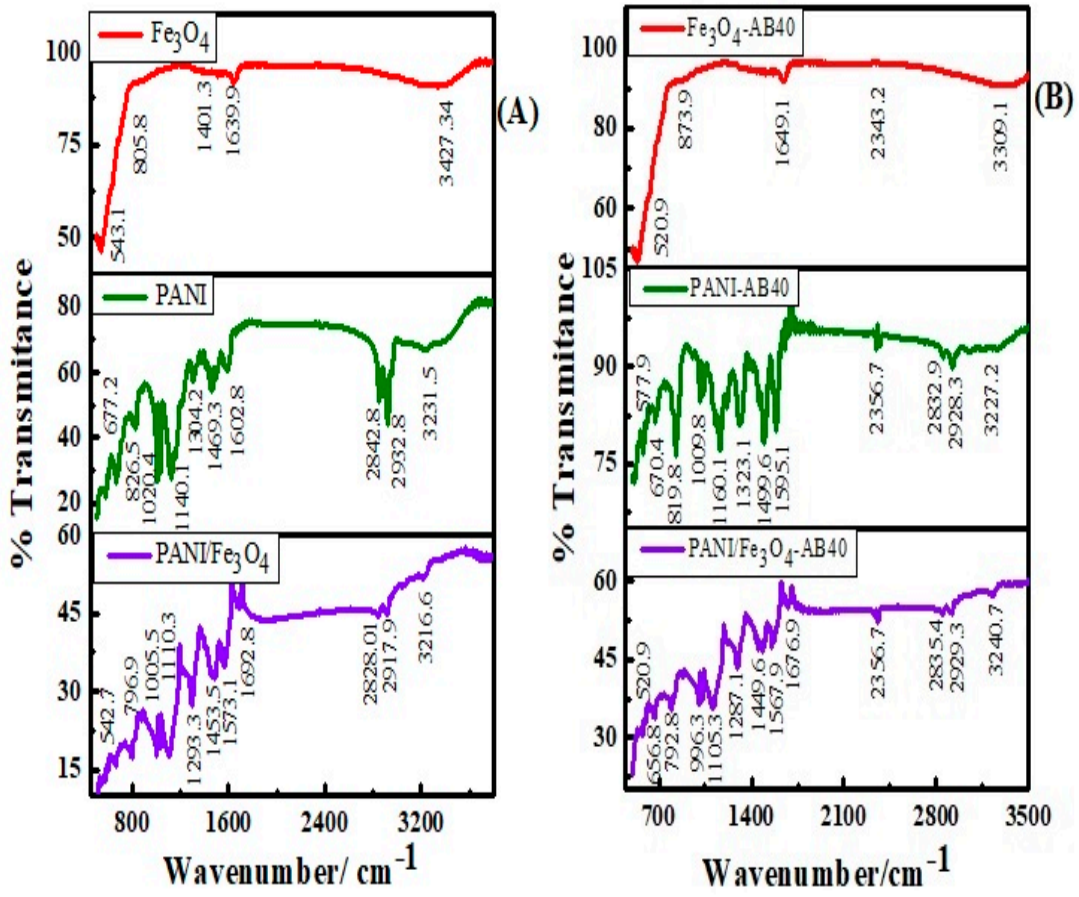

Figure 4. FTIR spectra of Fe_3O_4, PANI and PANI/ Fe_3O_4 composites before (**A**) and after (**B**) the adsorption of AB40.

3.1.4. Surface Area Study

The surface area of adsorbent plays a unique role in the adsorption study. The Brunauer–Emmett–Teller (BET) technique was employed to determine the average pore size radius, pore volume and specific surface area of PANI, Fe_3O_4 and PANI/Fe_3O_4 composite via nitrogen adsorption–desorption analysis (Figure 5). The results obtained are summarized in Table 1. The data shows that specific surface area of PANI/Fe_3O_4 composite is greater than PANI and Fe_3O_4 particles [69]. After the adsorption of AB40, the surface area of Fe_3O_4, PANI and PANI/Fe_3O_4 composite decreases [70]. However, the extent of reduction is more for PANI as compared to Fe_3O_4 and PANI/Fe_3O_4 composites, showing a greater adsorption of the dye on PANI.

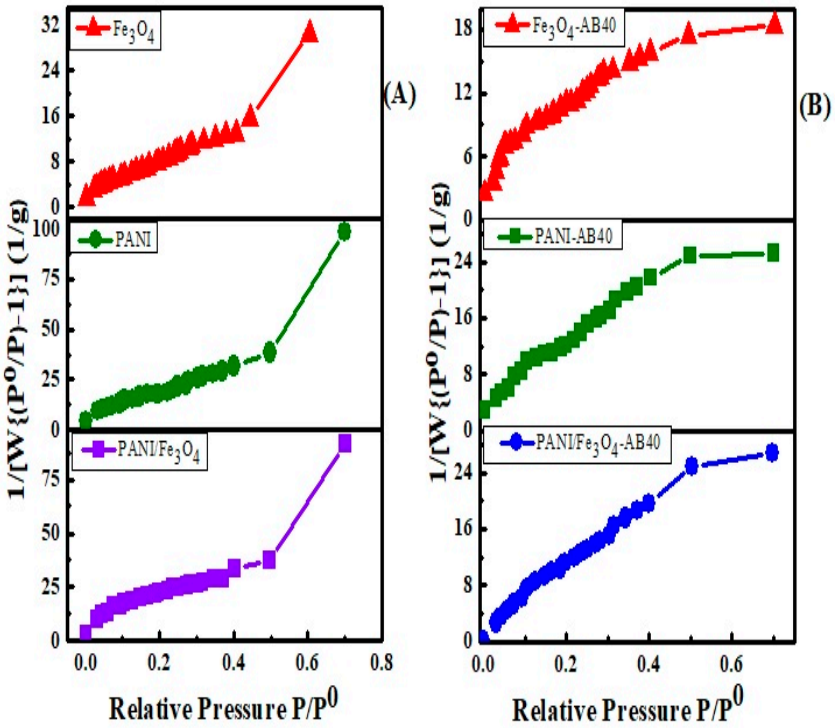

Figure 5. Brunauer–Emmett–Teller (BET) surface area of Fe_3O_4, PANI and PANI/Fe_3O_4 composites before (**A**) and after (**B**) the adsorption of AB40.

Table 1. Surface area, average pore volume and pore radius of PANI, Fe_3O_4 and PANI/Fe_3O_4 composites.

Status	Materials	Surface Area (m^2/g)	BJH Average Pore Radius (A^0)	BJH Pore Volume (cc/g)
Before adsorption	Fe_3O_4	71.314	15.749	0.053
	PANI	95.423	16.565	0.049
	PANI/Fe_3O_4	98.184	15.501	0.069
After adsorption	Fe_3O_4-AB40	53.707	13.334	0.033
	PANI-AB40	43.938	11.743	0.043
	PANI/Fe_3O_4-AB40	65.269	12.804	0.036

3.2. Isotherms Study

The most important step in the adsorption study is the fitting of adsorption isotherm models to adsorption data in order to describe how interaction occurs between adsorbent and dye. A number of adsorption isotherms are available and have been successfully applied by the earlier researcher to analyze the adsorption data [71]. In this study, four adsorption isotherms models, namely Freundlich, Tempkin, Langmuir and Dubinin–Radushkevich (D–R) were tested. Adsorption parameters so calculated have been summarized in Table 2. The correlation factor R^2, indicates that Freundlich adsorption isotherm equation fit more closely to the adsorption data. The linearized form of Freundlich adsorption equation is expressed in Equation (2);

$$\ln q_e = \ln k_f + \frac{1}{n}\ln c_e \quad (2)$$

where q_e (mg g^{-1}) and C_e (mg L^{-1}) are the solid and liquid phase equilibrium concentration of dye. K_f is constant, and is known as the Freundlich constant and $1/n$ is the slope obtained by plotting $\ln q_e$ vs. C_e shown in Figure 6A. The values of $1/n$ vary due to heterogeneity of the adsorbing materials.

The values of $1/n$ shows favorable ($0 < 1/n < 1$), unfavorable ($1/n > 1$) or irreversible ($1/n = 0$) adsorption. However, if its value is unity, the system is at equilibrium and will show heterogeneity [72]. In the present work, the values of $1/n$ calculated from Freundlich for Fe_3O_4, PANI and PANI/Fe_3O_4 composites are 0.126, 0.504 and 0.723 respectively showing favorable physical adsorption [73].

Table 2. Summary of parameters calculated from adsorption isotherms models.

Adsorbents	Adsorption Isotherms												
	Freundlich			Langmuir				Tempkin			D-R		
	1/n	Kf	R^2	q_{max}	K_L	R_L	R^2	ß$_T$	K_T	R^2	q_S	E_{ads}	R^2
Fe_3O_4	0.126	22.88	0.933	130.5	0.195	0.059	0.499	26.38	3.050	0.917	98.83	3.199	0.933
PANI	0.504	98.21	0.971	264.9	1.579	0.339	0.773	14.24	153.6	0.957	166.7	23.63	0.971
PANI/Fe_3O_4	0.723	58.99	0.946	216.9	0.499	0.167	0.859	22.15	14.17	0.902	134.5	11.29	0.909

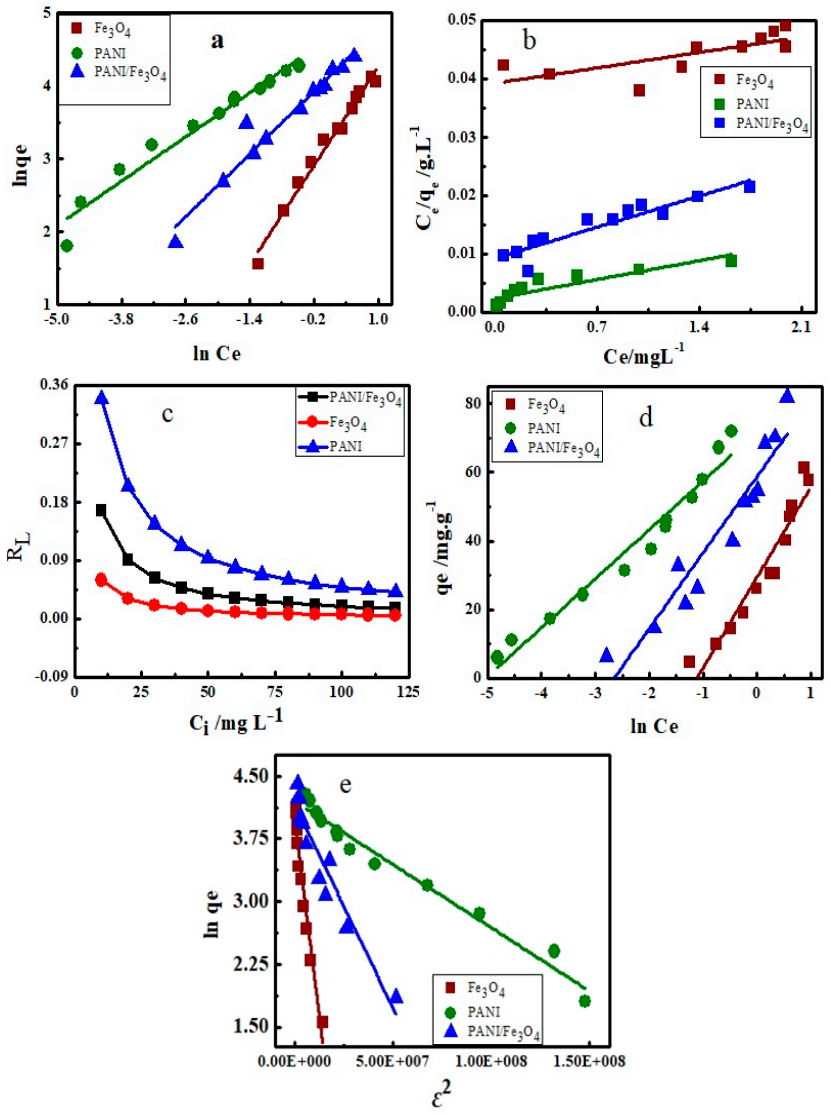

Figure 6. The Isotherm plots (**a**) Freundlich, (**b**) Langmuir, (**c**) Separation factor, (**d**) Tempkin and (**e**) D–R of adsorption of AB40 on Fe_3O_4, PANI and PANI/Fe_3O_4 composite.

The data were also fitted in the Langmuir adsorption isotherm equation (Equation (3)) as shown below;

$$\frac{c_e}{q_e} = \frac{1}{q_{max}k_L} + \frac{1}{q_{max}}c_e \quad (3)$$

where C_e (mg L^{-1}) and q_e (mg g^{-1}) indicates the concentration of dye and amount of dye adsorbed per gram of adsorbent at equilibrium, respectively. Similarly, K_L (mg L^{-1}) represent the Langmuir constant related to adsorption energy and q_{max} (mg g^{-1}) is the maximum adsorption capacity of adsorbing materials which can be calculated from the slope. The maximum adsorption capacity of AB40 onto Fe_3O_4, PANI and PANI/Fe_3O_4 composites are 130.5, 264.9 and 216.9 mg g^{-1}, respectively, as compared in Table 3A. The dimensionless constant (R_L) also called separation factor, expresses essential features of the Langmuir isotherm and is represented by Equation (3a).

$$R_L = \frac{1}{(1 + K_L C_i)} \tag{3a}$$

where C_i (mg L^{-1}) is the initial concentration of AB40. Values of R_L indicate that isotherm is either favorable ($1 > R_L > 0$), linear ($R_L = 1$), irreversible ($R_L = 0$) or unfavorable ($1 < R_L$) [74]. In the present study, the values of R_L range from 0.00525 to 0.34988 as depicted in Figure 6c, which shows that adsorption of AB40 onto Fe_3O_4, PANI and PANI/Fe_3O_4 composites is favorable at low concentration [75].

Table 3. Kinetics parameters for adsorption of AB40 on Fe_3O_4, PANI and PANI/Fe_3O_4 composite based on pseudo-first-order and pseudo-second-order equations.

	Pseudo 1st Order			**Pseudo 2nd Order**		
Adsorbents	**K_1 (min^{-1})**	**qe (mg g^{-1})**	**R^2**	**K_2 (g mg^{-1} min^{-1})**	**qe (mg g^{-1})**	**R^2**
Fe_3O_4	-0.015	1.765	0.812	0.0665	126.3	0.999
PANI	-0.033	4.823	0.885	0.0028	258.8	0.983
PANI/ Fe_3O_4	-0.047	2.495	0.881	0.0213	207.3	0.994

The Tempkin isotherm is also an important isotherm model and has been used by researchers to analyze their adsorption data [76,77]. The Tempkin isotherm assumes that due to interactions of the dye with the adsorbent, the adsorption decreases linearly and is characterized by binding energies. It is represented by the following equation (Equation (4));

$$q_e = \beta \ln k_T + \beta \ln c_e \tag{4}$$

where C_e (mg L^{-1}), q_e (mg g^{-1}) and K_T (L g^{-1}) are equilibrium concentration, equilibrium adsorption and binding constant at equilibrium. It is obtained by plotting q_e vs. lnC_e (Figure 6d). The constant β, considers the interaction between adsorbent and dye (Equation (4a)).

$$\beta = \frac{RT}{b} \tag{4a}$$

where b is the Tempkin isotherm constant of binding energy (J $mol^{-1}K^{-1}$). The correlation factors (R^2) given in Table 2 show that the Tempkin isotherm also fit the adsorption data. The values of K_T show that there is strong interaction between AB40 and PANI as compared to Fe_3O_4 and PANI/Fe_3O_4 composites (Table 2).

Dubinin–Radushkevich (D–R) as expressed in Equation (5) was also fitted to the adsorption data.

$$\ln q_e = \ln q_s - \beta \varepsilon^2 \tag{5}$$

where q_e is the amount of dye in mg adsorbed per gram of adsorbent (mg g^{-1}), β (mol^2 $K^{-1}J^{-2}$) is the activity coefficient useful in obtaining the mean adsorption energy E_{ad} (kJ mol^{-1}), q_s is the adsorption maximum, and ε is Polanyi potential. ε and E_{ad} are expressed by Equations (5a) and (5b) respectively.

$$\varepsilon = RT \ln\left(1 + \frac{1}{c_e}\right) \tag{5a}$$

$$E_{ad} = \frac{1}{\sqrt{1 - 2\beta}} \quad (5b)$$

where R is the gas constant which has a value of 8.314 (J mol^{-1} K^{-1}) and T is the kelvin temperature.

D–R adsorption model is a unique model used to differentiate between the chemical and physical adsorption on the basis of adsorption energy. In early research, it has been demonstrated that if the value of adsorption energy is less than 40 kJ mol^{-1}, the adsorption is physical [78]. In the present work, the values of E_{ad}, calculated by the Equation (5b) are less than 40 kJ mol^{-1} for adsorption of AB40 and PANI as compared to Fe_3O_4 and PANI/Fe_3O_4 composites showing physical adsorption as shown in Table 2.

3.3. Effect of Contact Time and Temperature on Adsorption

The contact time between adsorbent and dye is of great interest in the adsorption process. The optimum time of equilibrium was determined by adding 0.0340 ± 0.0001 g of each Fe_3O_4, PANI and PANI/Fe_3O_4 composite to 20 mL of AB40 (50 mg L^{-1}) in a series of experiments and was shacked at 150 rpm at 30 °C. The adsorption data so obtained was plotted as a function of time (Figure 7a). The graph shows that adsorption is very fast in the initial 10–15 min. The initial fast adsorption is due to a strong interaction between active sites of adsorbents and dye molecules. After 40–50 min, adsorption rate of dye become constant due to filling of active sites on the surface of adsorbents. This time period is defined as the dynamic equilibrium time. At the equilibrium time, rate of adsorption and desorption occurs simultaneously with the same speed [79]. Maximum adsorption of AB40 on Fe_3O_4, PANI and PANI/Fe_3O_4 composite is observed at 30 °C indicating exothermic nature (Figure 7b).

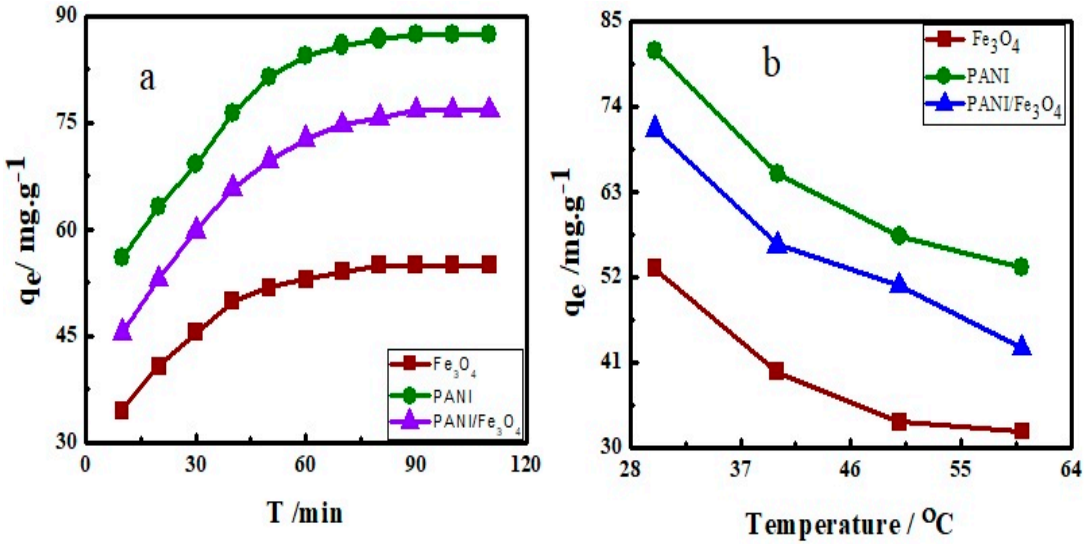

Figure 7. Effect of (**a**) time and (**b**) temperature on adsorption of AB40 onto Fe_3O_4, PANI and PANI/Fe_3O_4 composite.

3.4. Effect of pH on Adsorption

The pH of the dye solution plays a unique role in adsorption process. In the present work, the effect of pH on adsorption was investigated between 2–12. Results so obtained are plotted as adsorption versus pH (Figure 8). The plot indicates that adsorption of AB40 is high in acidic medium on all three adsorbents. When at a low pH, the backbone of adsorbents is positively charged and the active sites like Fe–O and –C=N are protonated. These positively charged sites have a strong interaction with the negatively charged sites of AB40 dye and hence enhance the adsorption. On the other hand, in a basic medium, the deprotonation of Fe–O–H and –C–N–H will create a negative charge in these groups which will repel the negatively charged sites of dye electrostatically, thus adsorption reduces [80].

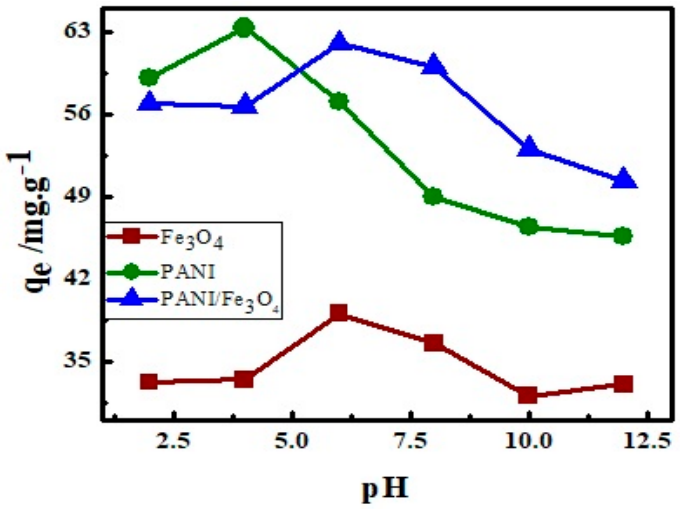

Figure 8. The effect of solution pH on adsorption of AB40 on PANI, Fe_3O_4 and PANI/Fe_3O_4 composite.

3.5. Effect of Ionic Strength on Adsorption

The effluent of industrial water also contains several ions. Therefore, the presence of these ions will also affect the adsorption process. In the present study, ionic strength effect of sodium sulfate and calcium chloride on adsorption has been studied in the pH between 5–6. The adsorption data so obtained are plotted against ionic strength (Figure 9). The plots (Figure 9a,b) show that adsorption of AB40 on PANI, Fe_3O_4 and PANI/Fe_3O_4 composite increases with an increase in ionic strength. This can be attributed to the fact that when both dye and adsorbent have similar charges, an increase in ionic strength will increase adsorption. This effect is more prominent in the adsorption of AB40 on PANI/Fe_3O_4 composite as compared to pristine PANI, because PANI/Fe_3O_4 composite contains a greater number of sites with a lone pair of electrons which behave as negatively charged groups [81]. Moreover, the significant increase in the adsorption of AB40 by increasing the ionic strength can be attributed to the dimerization of dye. A number of intermolecular forces like dipole-dipole, ion-dipole and Van der Waals forces have been suggested as the cause of the dimerization. Alberghina and co-workers have observed such type of dimerization while studying salts and temperature effect on adsorption of reactive dyes onto activated carbon [51].

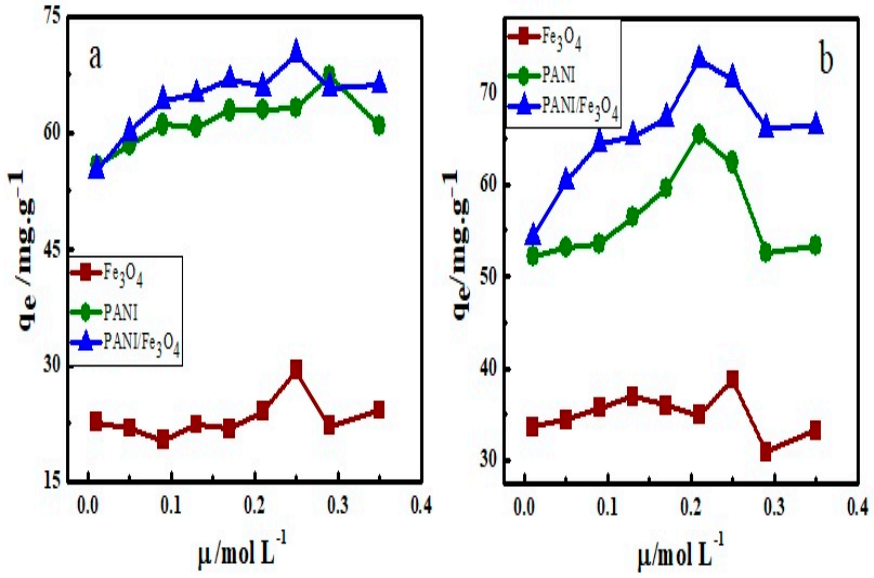

Figure 9. The effect of ionic strength of (**a**) $Na_2SO_4.7H_2O$ and (**b**) $CaCl_2.2H_2O$ on adsorption of AB40 onto Fe_3O_4, PANI and PANI/Fe_3O_4 composite.

3.6. Effect of Adsorbent Dosage on Adsorption

To investigate the effect of adsorbent dosage on adsorption, 0.034, 0.045, 0.075 and 0.1 g of each Fe_3O_4, PANI and PANI/Fe_3O_4 composite were added to 100 mg L^{-1} of AB40 separately and shook at 150 rpm at 30 °C and the amount adsorbed was noted (Figure 10). An increase in the adsorption of dye was observed by increasing the adsorbent dose. Initially the rate of adsorption is fast due to greater number of active site and splitting effect of the flux between adsorbents and dye [82].

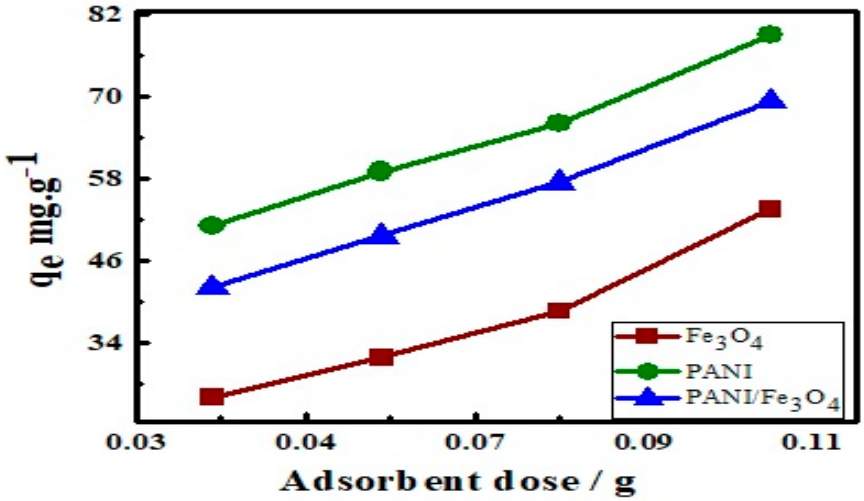

Figure 10. Effect of adsorbent dosage on adsorption of AB40 onto Fe_3O_4, PANI and PANI/Fe_3O_4 composite.

3.7. Adsorption Kinetics

Four kinetic equations namely pseudo 1st order, pseudo 2nd order, Elovich model and intra-particle diffusion models were used to analyze the adsorption data. The relationship between the amount of dye adsorbed on adsorbents and adsorption time was determined. Pseudo-first-order and pseudo-second-order equations are expressed in Equations (6) and (7) respectively as below;

$$\ln(q_e - q_t) = \ln q_e - k_1 t \quad (6)$$

$$\frac{t}{q_t} = \frac{1}{k_2 q_e^2} + \frac{t}{q_e} \quad (7)$$

where q_e (mg g^{-1}) is the equilibrium adsorption and q_t (mg g^{-1}) is the amount of dye adsorbed after time t (min). K_1 (min^{-1}) and K_2 (g mg^{-1} min^{-1}) are the rate constants of pseudo-first-order and pseudo-second-order equations respectively.

The Elovich kinetic model can be expressed as shown below in Equation (8);

$$q_t = \frac{1}{\beta}\ln(\alpha\beta) + \frac{1}{\beta}\ln t \quad (8)$$

where α (mg g^{-1} min^{-1}) shows an initial rate of adsorption and β (mg g^{-1}) is the desorption constant relating to the activation energy and the extent of surface coverage.

Intra-particle diffusion model is expressed in Equation (9);

$$q_t = k_d t^{1/2} + c \quad (9)$$

where K_d (g mg^{-1} $min^{-1/2}$) represent the rate of diffusion constant and C (mg g^{-1}) is the constant of boundary layer thickness.

The fitted curves of adsorption of AB40 onto Fe_3O_4, PANI and PANI/Fe_3O_4 composites are shown in Figure 11. The parameters of kinetics are summarized in Tables 3 and 4. The correlation factor of pseudo-first-order (R^2), are 0.812, 0.885 and 0.881 for adsorption of AB40 onto Fe_3O_4, PANI and PANI/Fe_3O_4 composites. These values indicate that adsorption of AB40 does not follow pseudo-first-order kinetics [83]. Similarly R^2 of Elovich model for PANI/Fe_3O_4 composites is 0.707 and intra-particle diffusion model for Fe_3O_4 is 0.864 indicating that these models also do not fit well for the adsorption data of AB40 on all of the three adsorbents [84]. R^2 values of pseudo-second-order equation show that the adsorption kinetics are more accurately described by this model (Table 3). Moreover, the q_e values calculated by the pseudo-second-order equation agree more closely with the adsorption isotherm values [85].

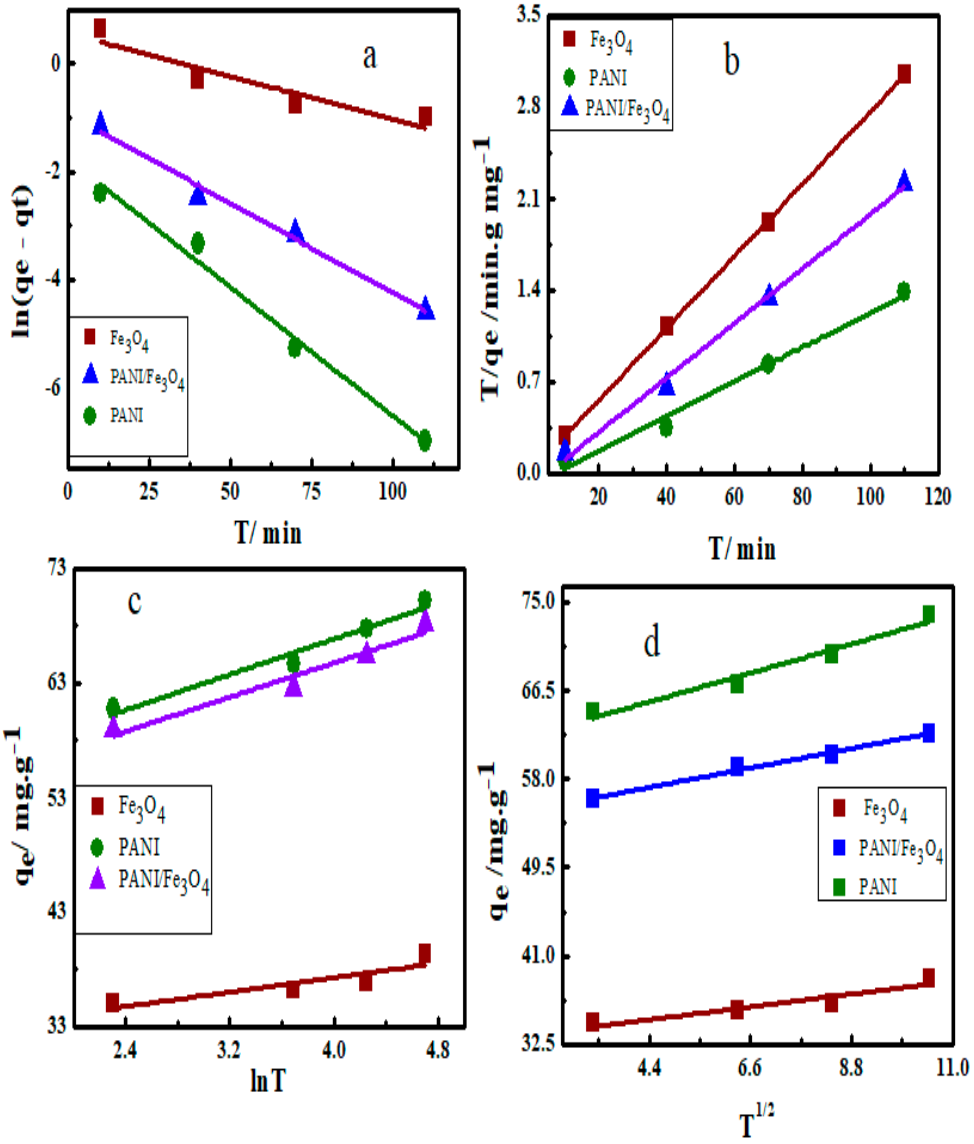

Figure 11. The Kinetics model (**a**) pseudo-first-order, (**b**) pseudo-second-order, (**c**) Elovich model and (**d**) intra-particle diffusion model for adsorption of AB40 on Fe_3O_4, PANI and PANI/Fe_3O_4 composite.

Table 4. Kinetics parameters for adsorption of AB40 on Fe_3O_4, PANI and PANI/Fe_3O_4 composite with Elovich model and intra-particle diffusion model.

	Elovich Model			Intra Particle Diffusion Model		
Adsorbents	**α (mg g^{-1}min^{-1})**	**β (g mg^{-1})**	**R^2**	**k_d (g mg^{-1}min$^{-1/2}$)**	**C (mg g^{-1})**	**R^2**
Fe_3O_4	131.9	0.258	0.911	0.556	32.45	0.864
PANI	439.8	0.637	0.929	1.257	61.89	0.916
PANI/ Fe_3O_4	378.7	0.267	0.707	0.847	53.47	0.917

3.8. Adsorption Mechanism

Two routes can be proposed for the adsorption of AB40 on the surface of PANI salt and PANI/Fe_3O_4 composite. In the first one, electrostatic interaction may occur between the molecules of AB40 and PANI. The second one involves the formation of an H-bond between the dye and –NH group of PANI. H-bond formation is also possible between AB40 and –OH group present on the surface of Fe_3O_4.

The electrostatic interactions are based on the fact that when dye is dissolved in water it splits into positively and negatively charged ions (Dye-SO_3^-). These negatively charged anions (Dye-SO_3^-) interact with positively charged sites (–$^+$NH–) on PANI surface. The enhancement of dye adsorption in acidic medium is good evidence of electrostatic interaction expressed in Section 3.4. Existence of physical forces (H-bond) is also supported by FTIR spectra shown in Figure 4B. After adsorption of AB40, all peaks in the spectra of PANI and PANI/Fe_3O_4 composite are shifted towards low-frequency values. Moreover, appearance of peak at 2356.7 cm^{-1} shows existence of AB40 adheres to the surface of PANI and PANI/Fe_3O_4 composites [72].

3.9. Thermodynamics of Adsorption

The nature of adsorption can be described well with thermodynamic parameters like Gibbs free energy, change in enthalpy and change in entropy. Values of Gibbs free energy were calculated by the equation shown below (Equation (10));

$$\Delta G = -RT\ln K_e \tag{10}$$

where K_e is the equilibrium constant, R is the gas constant having the value of 8.314 J K^{-1} mol^{-1} and T represents the Kelvin temperature. The negative sign of ΔG values shows that the adsorption of AB40 onto Fe_3O_4, PANI and PANI/ Fe_3O_4 composites are spontaneous (Table 5). The values of ΔG which range from −20 to zero kJ mol^{-1} show physical adsorption [47]. The values of ΔH and ΔS were calculated from the slope and intercept of van't Hoff equation respectively by plotting lnk_e vs. 1/T (Figure 12b). The van't Hoff equation is expressed as below;

$$\ln K_e = -\frac{\Delta H}{RT} + \frac{\Delta S}{R} \tag{11}$$

$$K_e = \frac{q_e}{c_e} \tag{11a}$$

where q_e (mg g^{-1}) is the adsorption maximum and C_e (mg L^{-1}) is the concentration of dye at equilibrium. The negative values of ΔH and ΔS shown in Table 4 show that adsorption is exothermic and correlate to the effect of temperature on adsorption expressed in Section 3.3. Activation energy also expresses the nature of adsorption. Its values are calculated from the slope of Arrhenius equation by plotting lnK vs. 1/T shown in Figure 12b. The Arrhenius equation is expressed as below;

$$\ln k = \ln A - \frac{Ea}{RT} \tag{12}$$

where K is the rate constant, A is Arrhenius constant, Ea is the activation energy, R is the general gas constant and T is kelvin temperature. The activation energy of adsorption of AB40 onto Fe_3O_4, PANI and PANI/Fe_3O_4 composites are 30.12, 22.09 and 26.13 kJ mol^{-1} showing physical adsorption. Ozcan and co-workers have demonstrated that physical adsorption is characterized by the activation energy values range from 5 to 40 kJ mol^{-1} and its higher values (40–800) kJ mol^{-1} express chemical adsorption [85].

Table 5. Activation energy and thermodynamic parameters of AB40 adsorption.

Adsorbents	ΔH (kJ mol^{-1})	ΔS (kJ mol^{-1})	ΔG (kJ mol^{-1})	Ea (kJ mol^{-1})
Fe_3O_4	−6.077	−0.026	−11.93	30.12
PANI	−8.993	−0.032	−19.87	22.09
PANI/Fe_3O_4	−10.62	−0.054	−19.75	26.13

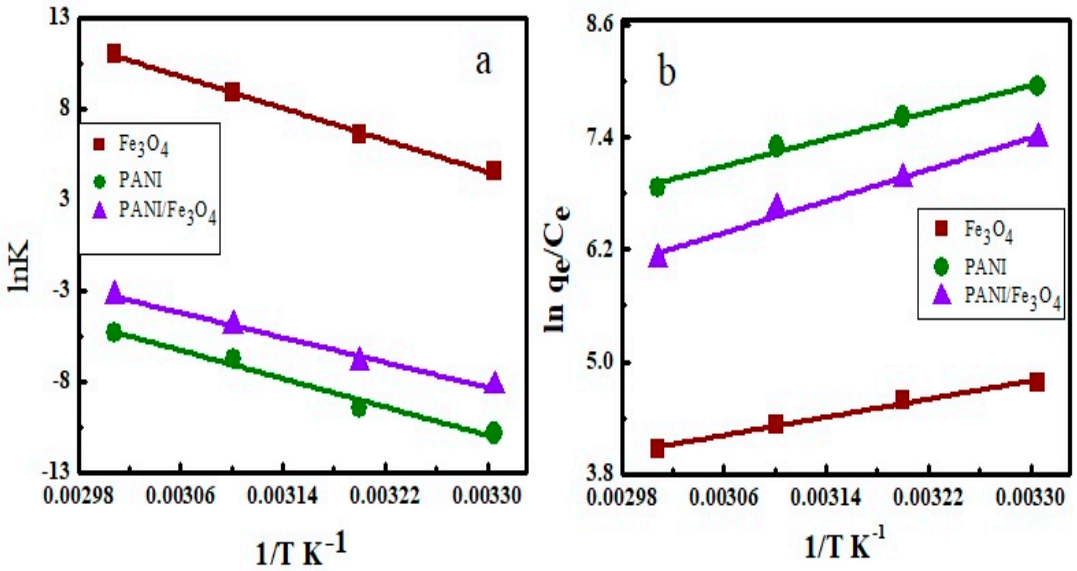

Figure 12. (**a**) Arrhenius plot and (**b**) van't Hoff plot for calculation of activation energy and thermodynamic parameters.

4. Conclusions

PANI, Fe_3O_4 and their composite can effectively be utilized for the removal of AB40 dye from aqueous environment. The comparison of adsorption behavior of the three materials for the uptake of AB40 reveals that the dye interaction with PANI was higher than both Fe_3O_4 and composites materials. This enhancement in adsorption on PANI can be attributed to the electrostatic interaction between oppositely charged sites of PANI and AB40. Greater number of active sites leading to physical forces also enhanced the adsorption of dye on PANI. In case of PANI/Fe_3O_4 composites the lone pair electrons present on the oxygen causes repulsive interaction with the negatively charged dye and reduces the adsorption. This fact was confirmed in the effect of ionic strength on adsorption where PANI/Fe_3O_4 composites showed higher adsorption than pristine PANI. The maximum amount of dye adsorbed on PANI, Fe_3O_4 and PANI/Fe_3O_4 composites were 264.9, 130.5 and 216.9 mg g^{-1}, respectively. The enhancement of adsorption on PANI was also supported by its smaller value of activation energy than Fe_3O_4 and PANI/Fe_3O_4 composites. Freundlich adsorption isotherm model fitted more closely with the adsorption data. The adsorption was high in acidic conditions and followed pseudo-second-order kinetics. The negative sign of the values of enthalpy changes, entropy changes and Gibbs free energy changes confirmed spontaneous and exothermic nature of adsorption.

Supplementary Materials: The following are available online at http://www.mdpi.com/1996-1944/12/18/2854/s1, Figure S1: UV-Visible calibration curve of AB40.

Author Contributions: A.M. wrote the original draft and executed all the experiments. A.u.H.A.S. supervised. A.u.H.A.S. and S.B. contributed to writing and corrected and edited the manuscript.

Funding: This research was funded by the Higher Education Commission Pakistan (project No. 20-1647 and 20–111/NRPU/R&D/HEC). The APC was funded by the German Research Foundation and the Open Access Publication Funds of the Technische Universität Braunschweig.

Acknowledgments: We acknowledge support from the German Research Foundation and the Open Access Publication Funds of the Technische Universität Braunschweig. S.B. wants to thank the Alexander von Humboldt Foundation Germany for support.

Conflicts of Interest: The authors declare no conflict of interest.

References

1. Bhadraa, S.; Khastgir, D.; Singhaa, N.K.; Leeb, J.H. Progress in preparation, processing and applications of polyaniline. *Prog. Polym. Sci.* **2009**, *34*, 783–810. [CrossRef]
2. Kiskan, B.; Yagci, Y. Synthesis and characterization of thermally curable polyacetylenes by polymerization of propargyl benzoxazine using rhodium catalyst. *Polymer* **2008**, *49*, 2455–2460. [CrossRef]
3. Shah, A.-U.-H.A.; Kamran, M.; Bilal, S.; Ullah, R. Cost Effective Chemical Oxidative Synthesis of Soluble and Electroactive Polyaniline Salt and Its Application as Anticorrosive Agent for Steel. *Materials* **2019**, *12*, 1527. [CrossRef] [PubMed]
4. Del Valle, M.A.; Diaz, F.R.; Armijo, F.; Soto, P. Electro-synthesis and characterization of polythiophene nano-wires/platinum nano-particles composite electrodes. Study of formic acid electro-catalytic oxidation. *Electrochim. Acta* **2012**, *71*, 277–282. [CrossRef]
5. Shen, C.; Sun, Y.; Yao, W.; Lu, Y. Facile synthesis of polypyrrole nanospheres and their carbonized products for potential application in high-performance supercapacitors. *Polymer* **2014**, *55*, 2817–2824. [CrossRef]
6. Fahim, M.; Shah, A.H.A.; Bilal, S. Highly stable and efficient performance of binder free symmetric supercapacitor fabricated with electroactive polymer synthesized via interfacial polymerization. *Materials* **2019**, *12*, 1626. [CrossRef] [PubMed]
7. Ganesan, R.; Shanmugam, S.; Gedanken, A. Pulsed sonoelectrochemical synthesis of polyaniline nanoparticles and their capacitance properties. *Synth. Met.* **2008**, *158*, 848–853. [CrossRef]
8. Kulkarni, S.B.; Joshi, S.S.; Lokhande, C.D. Facile and efficient route for preparation of nanostructured polyaniline thin films: Schematic model for simplest oxidative chemical polymerization. *Chem. Eng. J.* **2011**, *166*, 1179–1185. [CrossRef]
9. Vivekanandan, J.; Ponnusamy, V.; Mahudeswaran, A.; Vijayanand, P.S. Synthesis, characterization and conductivity study of polyaniline prepared by chemical oxidative and electrochemical methods. *Arch. Appl. Sci. Res.* **2011**, *3*, 147–153.
10. Xu, P.; Singh, A.; Kaplan, D.L. Enzymatic Catalysis in the Synthesis of Polyanilines and Derivatives of Polyanilines. *Adv. Polym. Sci.* **2006**, *194*, 69–94.
11. Abdolahi, A.; Hamzah, E.; Ibrahim, Z.; Hashim, S. Synthesis of Uniform Polyaniline Nanofibers through Interfacial Polymerization. *Materials* **2012**, *5*, 1487–1494. [CrossRef]
12. Guo, X.; Fei, G.T.; Su, H.; Zhang, L.D. Synthesis of polyaniline micro/nanospheres by a copper(II)-catalyzed self-assembly method with superior adsorption capacity of organic dye from aqueous solution. *J. Mater. Chem.* **2011**, *21*, 8618. [CrossRef]
13. Lee, S.; Hong, J.Y.; Jang, J. Synthesis and electrical response of polyaniline/poly(styrene sulfonate)-coated silica spheres prepared by seed-coating method. *J. Colloid. Inter. Sci.* **2013**, *398*, 33–38. [CrossRef] [PubMed]
14. Zhang, Y.; Shao, Y.; Zhang, T.; Meng, G.; Wang, F. The effect of epoxy coating containing emeraldine base and hydrofluoric acid doped polyaniline on the corrosion protection of AZ91D magnesium alloy. *Corros. Sci.* **2011**, *53*, 3747–3755. [CrossRef]
15. Xu, W.; Zhao, K.; Niu, C.; Zhang, L.; Cai, Z.; Han, C.; He, L.; Shen, T.; Yan, M.; Qu, L. Heterogeneous branched core–shell SnO2–PANI nanorod arrays with mechanical integrity and three dimensional electron transport for lithium batteries. *Nano Energy* **2014**, *8*, 196–204. [CrossRef]
16. Farooq, S.; Tahir, A.; Krewer, U.; Shah, A.A.; Bilal, S. Efficient photocatalysis through conductive polymer coated FTO counter electrode in platinum free dye sensitized solar cells. *Electrochim. Acta* **2019**, *320*, 134544. [CrossRef]

17. Mujawar, S.H.; Ambade, S.B.; Battumur, T.; Ambade, R.B.; Lee, S.H. Electropolymerization of polyaniline on titanium oxide nanotubes for supercapacitor application. *Electrochim. Acta* **2011**, *56*, 4462–4466. [CrossRef]
18. Li, R.; Liu, L.; Yang, F. Preparation of polyaniline/reduced graphene oxide nanocomposite and its application in adsorption of aqueous Hg(II). *Chem. Eng. J.* **2013**, *229*, 460–468. [CrossRef]
19. Shen, J.; Shahid, S.; Amura, I.; Sarihan, A.; Mi Tian, M.; Emanuelsson, E.A. Enhanced adsorption of cationic and anionic dyes from aqueous solutions by polyacid doped polyaniline. *Synth. Met.* **2018**, *245*, 151–159. [CrossRef]
20. Huang, Y.; Li, J.; Chen, X.; Wang, X. Applications of conjugated polymer based composites in wastewater purification. *RSC Adv.* **2014**, *4*, 62160–62178. [CrossRef]
21. Lee, Y.M.; Nam, S.Y.; Ha, S.Y. Pervaporation of water/isopropanol mixtures through polyaniline membranes doped with poly(acrylic acid). *J. Membr. Sci.* **1999**, *159*, 41–46.
22. Bober, P.; Stejskal, J.; Trchováa, M.; Prokes, J. In-situ prepared polyaniline–silver composites: Single-and two-step strategies. *Electrochim. Acta* **2014**, *122*, 259–266. [CrossRef]
23. He, K.; Li, M.; Guo, L. Preparation and photocatalytic activity of PANI-CdS composites for hydrogen evolution. *Int. J. Hydrogen Energy* **2012**, *37*, 755–759. [CrossRef]
24. Yilmaz, H.; Zengin, H.S.; Unal, H.I. Synthesis and electrorheological properties of polyaniline/silicon dioxide composites. *J. Mater. Sci.* **2012**, *47*, 5276–5286. [CrossRef]
25. Wanga, J.G.; Yang, Y.; Huanga, Z.H.; Kang, F. Interfacial synthesis of mesoporous MnO2/polyaniline hollow spheres and their application in electrochemical capacitors. *J. Power Sources* **2012**, *204*, 236–243. [CrossRef]
26. Chandraa, S.; Lang, H.; Bahadur, D. Polyaniline-iron oxide nanohybrid film as multi-functional label-free electrochemical and biomagnetic sensor for catechol. *Anal. Chim. Acta* **2013**, *795*, 8–14. [CrossRef] [PubMed]
27. Vellakkat, M.; Kamath, A.; Raghu, S.; Chapi, S.; Hundekal, D. Dielectric Constant and Transport Mechanism of Percolated Polyaniline Nanoclay Composites. *Ind. Eng. Chem. Res.* **2014**, *53*, 16873–16882. [CrossRef]
28. Salem, M.A.; Salem, I.A.; Hanfy, M.G.; Ahmed, B.; Zak, A.B. Removal of titan yellow dye from aqueous solution by polyaniline/Fe3O4 nanocomposite. *Eur. Chem. Bull.* **2016**, *5*, 113–118.
29. Das, S.; Chakraborty, P.; Ghosh, R.; Paul, S.; Mondal, S.; Panja, A.; Nand, A.K. Folic Acid-Polyaniline Hybrid Hydrogel for Adsorption/Reduction of Chromium(VI) and Selective Adsorption of Anionic Dye from Water. *Chem. Eng.* **2017**, *5*, 9325–9337. [CrossRef]
30. Neuberger, T.; Schöpf, B.; Hofmann, H.; Hofmann, M.; Rechenberg, B. Superparamagnetic nanoparticles for biomedical applications: Possibilities and limitations of a new drug delivery system. *J. Magn. Magn. Mater.* **2005**, *293*, 483–496. [CrossRef]
31. Ito, A.; Shinkai, M.; Honda, H.; Kobayashi, T. Medical application of functionalized magnetic nanoparticles. *J. Biosci. Bioeng.* **2005**, *100*, 1–11. [CrossRef] [PubMed]
32. Pankhurst, Q.A.; Connolly, J.; Jones, S.K.; Dobson, J. Applications of magnetic nanoparticles in biomedicine. *J. Phys. D Appl. Phys.* **2003**, *36*, 167–181. [CrossRef]
33. Khurshid, H.; Hadjipanayis, C.; Chen, H.W.; Li, H.; Mao, H.; Machaidze, R.; Tzitzios, V.; Hadjipanay, G.C. Core/shell structured iron/iron-oxide nanoparticles as excellent MRI contrast enhancement agents. *J. Magn. Magn. Mater.* **2013**, *331*, 17–20. [CrossRef]
34. Wang, G.; Chang, Y.; Wang, L.; Wei, Z.; Kang, J.; Sang, L.; Dong, X.; Chen, G.; Wang, H.; Qi, H. Preparation and characterization of PVPI-coated Fe3O4 nanoparticles as an MRI contrast agent. *J. Magn. Magn. Mater.* **2013**, *340*, 57–60. [CrossRef]
35. Hyun Do, S.I.; Hoon Jo, Y.; Park, J.Y.; Hong, S.H. As3+removal by Ca–Mn–Fe3O4with and without H2O2: Effects ofcalcium oxide in Ca–Mn–Fe3O4. *J. Hazard. Mater.* **2014**, *280*, 322–330.
36. Hu, J.; Irene, M.C.; Chen, G. Fast Removal and Recovery of Cr(VI) Using Surface-Modified Jacobsite (MnFe2O4) Nanoparticles. *Langmuir* **2005**, *21*, 11173–11179. [CrossRef]
37. Aphesteguy, J.C.; Kurlyandskaya, G.V.; de Celis, J.P.; Safronov, A.P.; Schegoleva, N.N. Magnetite nanoparticles prepared by co-precipitation method in different conditions. *Mater. Chem. Phys.* **2015**, *161*, 243–249. [CrossRef]
38. Amer, M.A.; Meaz, T.M.; Attalah, S.S.; Ghoneim, A.I. Structural and magnetic characterization of the Mg0.2_xSrxMn0.8Fe2O4 nanoparticles. *J. Magn. Magn. Mater.* **2014**, *363*, 60–65. [CrossRef]
39. Lam, U.T.; Mammucari, R.; Suzuki, K.; Foster, N.R. Processing of iron oxide nanoparticles by supercritical fluids. *Ind. Eng. Chem. Res.* **2008**, *47*, 599–614. [CrossRef]
40. Tavakoli, A.; Sohrabi, M.; Kargari, A. A review of methods for synthesis of nano structured metals with emphasis on iron compounds. *Chem. Pap.* **2007**, *61*, 151–170. [CrossRef]

41. Teja, A.S.; Koh, P. Y Synthesis, properties, and applications of magnetic iron oxide nanoparticles. *Prog. Cryst. Growth Charact. Mater.* **2009**, *55*, 22–45. [CrossRef]
42. Majewski, P.; Thierry, B. Functionalized magnetite nanoparticles synthesis, properties, and bio-applications. *Solid State Mater. Sci.* **2007**, *32*, 203–215. [CrossRef]
43. Jia, Z.; Yujun, W.; Yangcheng, L.; Jingyu, M.; Guangsheng, L. In situ preparation of magnetic chitosan/Fe3O4 composite nanoparticles in tiny pools of water-in-oil microemulsion. *React. Funct. Polym.* **2006**, *66*, 1552–1558.
44. Khan, A.; Aldwayyan, A.S.; Alhoshan, M.; Alsalhi, M. Synthesis by in situ chemical oxidative polymerization and characterization of polyaniline/iron oxide nanoparticle composite. *Polym. Int.* **2010**, *59*, 1690–1694. [CrossRef]
45. Rasha, M.K. Synthesis, characterization, magnetic and electrical properties of the novel conductive and magnetic Polyaniline/MgFe2O4 nanocomposite having the core–shell structure. *J. Alloys Compounds* **2011**, *509*, 9849–9857.
46. Bhaumik, M.; Choi, H.J.; McCrindle, R.I.; Maity, A. Composite nanofibers prepared from metallic iron nanoparticles and polyaniline: High performance for water treatment applications. *J. Colloid. Interface Sci.* **2014**, *425*, 75–82. [CrossRef] [PubMed]
47. Mohamed, A.S. The role of polyaniline salts in the removal of direct blue 78 from aqueous solution: A kinetic study. *React. Funct. Polym.* **2010**, *70*, 707–714.
48. Cui, H.; Qian, Y.; Li, Q.; Zhang, Q.; Zhai, J. Adsorption of aqueous Hg(II) by a polyaniline/attapulgite composite. *Chem. Eng. J.* **2012**, *211*, 216–223.
49. Muhammad, A.; Shah, A.H.A.; Bilal, S.; Rahman, G. Basic Blue Dye Adsorption from Water using Polyaniline/Magnetite(Fe3O4) Composites: Kinetic and Thermodynamic Aspects. *Materials* **2019**, *12*, e1764. [CrossRef]
50. Keyhanian, F.; Shariati, S.; Faraji, M.; Hesabi, M. Magnetite nanoparticles with surface modification for removal of methyl violet from aqueous solutions. *Arab. J. Chem.* **2016**, *9*, 348–354. [CrossRef]
51. Patra, B.N.; Majhi, D. Removal of Anionic Dyes from Water by Potash Alum Doped Polyaniline: Investigation of Kinetics and Thermodynamic Parameters of Adsorption. *J. Phys. Chem. B* **2015**, *119*, 8154–8164. [CrossRef] [PubMed]
52. Hosseini, S.H.; Asadnia, A. Polyaniline/Fe3O4 coated on MnFe2O4 nanocomposite: Preparation, characterization, and applications in microwave absorption. *Int. J. Phys. Sci.* **2013**, *8*, 1209–1217.
53. Tung, L.M.; Cong, N.X.; Huy, L.T.; Lan, N.T.; Phan, V.N.; Hoa, N.Q.; Vinh, L.K.; Thinh, N.V.; Tai, L.T.; Ngo, D.T.; et al. Synthesis, Characterizations of Superparamagnetic Fe3O4–Ag Hybrid Nanoparticles and Their Application for Highly Eective Bacteria Inactivation. *J. Nanosci. Nanotechnol.* **2016**, *16*, 5902–5912. [CrossRef]
54. Bachan, N.; Asha, A.; Jeyarani, W.J.; Kumar, D.A.; Shyla, J.M. A Comparative Investigation on the Structural, Optical and Electrical Properties of SiO2–Fe3O4 Core–Shell Nanostructures with Their Single Components. *Acta Metall. Sin. Engl. Lett.* **2015**, *28*, 1317–1325. [CrossRef]
55. Bilal, S.; Gul, S.; Holze, R.; Shah, A.A. An impressive emulsion polymerization route for the synthesis of highly soluble and conducting polyaniline salt. *Synth. Met.* **2015**, *206*, 131–144. [CrossRef]
56. Hatamzadeh, M.; Ahar, M.J.; Jaymand, M. In Situ Chemical Oxidative Graft Polymerization of Aniline from Fe3O4 Nanoparticles. *Int. J. Nanosci. Nanotechnol.* **2012**, *8*, 51–60.
57. Akar, T.; Ozcan, A.S.; Tunali, S.; Ozcan, A. Biosorption of a textile dye (Acid Blue 40) by cone biomass of Thuja orientalis: Estimation of equilibrium, thermodynamic and kinetic parameters. *Bioresour. Technol.* **2008**, *99*, 3057–3065. [CrossRef] [PubMed]
58. Khoshsang, H.; Ghaffarinejad, A.; Kazemi, H.; Jabarian, S. Synthesis of Mesoporous Fe3O4 and Fe3O4/C Nanocomposite for Removal of Hazardous Dye from Aqueous Media. *J. Water Environ. Nanotechnol.* **2018**, *3*, 191–206.
59. Ballav, N.; Debnath, S.; Pillay, K.; Maity, A. Efficient removal of Reactive Black from aqueous solution usingpolyaniline coated ligno-cellulose composite as a potential adsorbent. *J. Mol. Liq.* **2015**, *209*, 387–396. [CrossRef]
60. Konicki, W.; Pełech, I.; Mijowska, E.; Jasinska, I. Adsorption of anionic dye Direct Red 23 onto magnetic multi-walled carbonnanotubes-Fe3C nanocomposite: Kinetics, equilibrium and thermodynamics. *Chem. Eng. J.* **2012**, *210*, 87–95. [CrossRef]

61. Sun, M.; Zhu, A.; Zhang, Q.; Liu, Q. A facile strategyto synthesize mono disperse super paramagnetic OA-modified Fe3O4 nanoparticles with PEG assistant. *J. Magn. Magn. Mater.* **2014**, *369*, 49–54. [CrossRef]
62. Asgari, S.; Fakhari, Z.; Berijanic, S. Synthesis and Characterization of Fe3O4 Magnetic Nanoparticles Coated with Carboxymethyl Chitosan Grafted Sodium Methacrylate. *J. Nanostruct.* **2014**, *4*, 55–63.
63. Ömeroglu Ay, C.; Özcan, A.S.; Erdogan, Y.; Özcan, A. Characterization of Punica granatum L. peels and quantitatively determination of its biosorption behavior towards lead(II) ions and Acid Blue 40. *Colloids Surf. B* **2012**, *100*, 197–204. [CrossRef] [PubMed]
64. Gul, H.; Shah, A.A.; Bilal, S. Fabrication of Eco-Friendly Solid-State Symmetric Ultracapacitor Device Based on Co-Doped PANI/GO Composite. *Polymers* **2019**, *11*, 1315. [CrossRef] [PubMed]
65. Kellenberger, A.; Dmitrieva, E.; Dunsch, L. Structure Dependence of Charged States in Linear Polyaniline as Studied by In Situ ATR-FTIR Spectroelectrochemistry. *J. Phys. Chem. B* **2012**, *116*, 4377–4385. [CrossRef] [PubMed]
66. Ding, S.; Mao, H.; Zhang, W. Fabrication of DBSA-Doped Polyaniline Nanorods by Interfacial Polymerization. *J. Appl. Polym. Sci.* **2008**, *109*, 2842–2847. [CrossRef]
67. Umare, S.S.; Shambharkar, B.H.; Ningthoujam, R.S. Synthesis and characterization of polyaniline–Fe3O4 nanocomposite: Electrical conductivity, magnetic, electrochemical studies. *Synth. Met.* **2010**, *160*, 1815–1821. [CrossRef]
68. Oppong, S.O.B.; Anku, W.; Shukla, S.K.; Govender, P. Lanthanum doped–TiO2 decorated on graphene oxide nanocomposite: A photocatalyst for enhanced degradation of acid blue 40 under simulated solar light. *Adv. Mater. Lett.* **2017**, *8*, 295–302. [CrossRef]
69. Ayad, M.; Zaghlol, S. Nanostructured crosslinked polyaniline with high surface area: Synthesis, characterization and adsorption for organic dye. *Chem. Eng. J.* **2012**, *204*, 79–86. [CrossRef]
70. Germain, J.; Frechet, J.M.; Svec, F. Hypercrosslinked polyanilines with nanoporous structure and high surface area: Potential adsorbents for hydrogen storage. *J. Mater. Chem.* **2007**, *17*, 4989–4997. [CrossRef]
71. Kegl, T.; Ban, I.; Lobnik, A.; Košak, A. Synthesis and characterization of novel γ-Fe2O3-NH4OH@SiO2(APTMS) nanoparticles for dysprosium adsorption. *J. Hazard. Mater.* **2019**, *378*, 120764. [CrossRef] [PubMed]
72. Javadian, H.; Angaji, M.T.; Naushad, M. Synthesis and characterization of polyaniline/g-alumina nanocomposite: A comparative study for the adsorption of three different anionic dyes. *J. Ind. Eng. Chem.* **2014**, *20*, 3890–3900. [CrossRef]
73. Crini, G. Kinetic and equilibrium studies on the removal of cationic dyes from aqueous solution by adsorption onto a cyclodextrin polymer. *Dyes Pigm.* **2008**, *77*, 415–426. [CrossRef]
74. Sharma, P.; Das, M.R. Removal of a Cationic Dye from Aqueous Solution Using Graphene Oxide Nanosheets: Investigation of Adsorption Parameters. *J. Chem. Eng. Data* **2013**, *58*, 151–158. [CrossRef]
75. Bhatt, A.S.; Sakaria, P.L.; Vasudevan, M.; Radheshyam, R.; Sudheesh, P.N.; Bajaj, H.C.; Mody, H.M. Adsorption of an anionic dye from aqueous medium by organoclays: Equilibrium modeling, kinetic and thermodynamic exploration. *RSC Adv.* **2012**, *2*, 8663–8671. [CrossRef]
76. Song, W.; Gao, B.; Xu, X.; Xing, L.; Han, S.; Duan, P.; Song, W.; Jia, R. Adsorption–desorption behavior of magnetic amine/Fe3O4functionalized biopolymer resin towards anionic dyes from wastewater. *Bioresour. Technol.* **2016**, *210*, 123–130. [CrossRef] [PubMed]
77. Mittal, A.; Mittal, J.; Malviya, A.; Gupta, V.K. Adsorptive removal of hazardous anionic dye "Congo red" from wastewaterusing waste materials and recovery by desorption. *J. Colloid Interface Sci.* **2009**, *340*, 16–26. [CrossRef]
78. Patil, M.R.; Khairnar, S.D.; Shrivastava, V.S. Synthesis, characterisation of polyaniline–Fe3O4 magnetic nanocomposite and its application for removal of an acid violet 19 dye. *Appl. Nanosci.* **2016**, *6*, 495–502. [CrossRef]
79. Abramian, L.; El-Rassy, H. Adsorption kinetics and thermodynamics of azo-dye Orange II onto highly porous titania aerogel. *Chem. Eng. J.* **2009**, *150*, 403–410. [CrossRef]
80. German-Heins, J.; Flury, M. Sorption of Brilliant Blue FCF in soils as affected by pH and ionic strength. *Geoderma* **2000**, *97*, 87–101. [CrossRef]
81. Alberghina, G.; Bianchini, R.; Fichera, M.; Fisichella, S. Dimerization of Cibacron Blue F3GA and other dyes: Influence of salts and temperature. *Dyes. Pigm.* **2000**, *46*, 129–137. [CrossRef]
82. Mahanta, D.; Madras, G.; Radhakrishnan, S.; Patil, S. Adsorption and Desorption Kinetics of Anionic Dyes on Doped Polyaniline. *J. Phys. Chem. B* **2009**, *113*, 2293–2299. [CrossRef] [PubMed]

83. Cao, J.S.; Lin, J.X.; Fang, F.; Zhang, M.T.; Hu, Z.R. A new absorbent by modifying walnut shell for the removal of anionic dye: Kinetic and thermodynamic studies. *Bioresour. Technol.* **2014**, *163*, 199–205. [CrossRef] [PubMed]
84. Weng, C.H.; Lin, Y.T.; Tzeng, T.W. Removal of Methylene Blue from Aqueous Solution by Adsorption onto Pineapple Leaf Powder. *J. Hazard. Mater.* **2009**, *170*, 417–424. [CrossRef]
85. Özcan, S.; Erdem, B.; Özcan, A. Adsorption of Acid Blue 193 from Aqueous Solutions Onto Na-Bentonite and DTMA-Bentonite. *J. Colloid Interface Sci.* **2004**, *280*, 44–54. [CrossRef] [PubMed]